ApoB100,LDLR$^{-/-}$ Mice Exhibit Reduced Electroretinographic Response and Cholesteryl Esters Deposits in the Retina

Lionel Bretillon,[1,2] *Niyazi Acar,*[1,2] *Mathias W. Seeliger,*[3] *Mylène Santos,*[1] *Marie Annick Maire,*[1] *Pierre Juanéda,*[1] *Lucy Martine,*[1] *Stéphane Grégoire,*[1] *Corinne Joffre,*[1] *Alain M. Bron,*[4,5] *and Catherine Creuzot-Garcher*[4,5]

Purpose. To evaluate the retinal phenotype of 7- and 14-month-old apoB100,LDLR$^{-/-}$ mice, a relevant animal model of lipid metabolism dysfunction.

Methods. Single-flash electroretinograms were obtained from 7- and 14-month-old apoB100,LDLR$^{-/-}$ and control mice fed a standard diet under both scotopic and photopic conditions. Visual cycle retinoids were analyzed in eyes from dark-adapted mice. Retinal and choroidal vascularization was evaluated with scanning laser ophthalmoscopy. Fatty acids were analyzed in the retina. Esterified and free cholesterol was detected in eye cryosections.

Results. Scotopic and photopic b-wave amplitudes were significantly reduced in apoB100,LDLR$^{-/-}$ mice compared with control mice at 7 and 14 months of age (between −25% and −35% in 7-month-old animals and between −50% and −60% in 14-month-old animals at 25 cds/m^2). Esterified cholesterol was found to accumulate at the basement of the retinal pigment epithelium in apoB100,LDLR$^{-/-}$ mouse eyes. On the contrary, no significant changes in the retinal profile of fatty acids and visual retinoids were observed in apoB100,LDLR$^{-/-}$ mice compared with control animals.

Conclusions. The exclusive expression of apoB100 in LDL receptor–null mouse altered the ERG profile, without modifying the visual cycle of retinoids and led to cholesterol deposition in the retina. These findings clearly suggest the role of cholesterol metabolism in the functioning of the retina and possibly in the etiology of ocular diseases, including age-related macular degeneration. (*Invest Ophthalmol Vis Sci.* 2008;49:1307–1314) DOI:10.1167/iovs.07-0808

Accumulation of lipids under the retinal pigment epithelium (RPE) and within Bruch's membrane (BrM) is a normal feature of aging[1,2] and has also been observed in human eyes with age-related maculopathy (ARM).[2,3] The mechanism of lipid deposition in sub-RPE is partly unknown but several hypotheses have emerged. Plasma lipids may infiltrate BrM.[4] Alternatively, lipid deposits may originate from abnormal RPE lipid metabolism involving apolipoprotein B (apoB)-rich lipoprotein synthesis.[2,5]

Insights have come from various mouse models of cardiovascular disease. C57Bl6 mice fed a high-fat diet and exposed to blue-green light develop basal laminar deposits,[6] characterized by unesterified cholesterol accumulation,[7] a histologic feature found in patients with ARM[3] or age-related macular degeneration (AMD).[8] The role of the low-density lipoprotein receptor (LDLR) has recently been highlighted in the transgenic LDLR knock out (LDLR$^{-/-}$) mouse model. After being fed a high-fat diet, LDLR$^{-/-}$ mice exhibited BrM abnormalities characterized by BrM thickening and deposition of translucent material[9] that may be lipid-rich particles comparable to the basal laminar deposits and drusen observed in patients with AMD.[10] The relative resistance of these mice to development of atherosclerotic lesions, unless they consume a high-cholesterol atherogenic diet,[11] has been attributed to the clearance of apoB48-lipoproteins by receptors other than LDLR, leading to lower plasma levels of LDL than can be expected from the lack of interaction between LDLR and apoB100, and subsequent lipoprotein clearance. Mice expressing exclusively apoB100 showed a modest increase in plasma LDL cholesterol but developed atherosclerosis[12,13] and basal laminar deposits in BrM[14] only after ingestion of an atherogenic diet. These features limit the usefulness of the LDLR$^{-/-}$ and apoB100 transgenic mice for studies on the role of LDLR and apoB100 in the context of an atherogenic diet, but fail to analyze the endogenous effect of pure LDL clearance deficiency independent of the increase in plasma lipid induced by the diet.

Transgenic mice lacking LDLR and expressing exclusively apoB100 have been established as a valuable model for atherosclerosis on a low-fat diet, with high plasma cholesterol levels and aortic atherosclerotic plaques.[15] These mice offer a unique opportunity to test the hypothesis that the lack of apoB100 and LDLR interaction alters lipid metabolism and impairs functioning of the retina. Therefore, we sought to analyze the electroretinographic profile, fundus images, and retinal and choroidal vasculature in 7- and 14-month-old apoB100,LDLR$^{-/-}$ mice, by comparison with control mice. In parallel, esterified and unesterified cholesterol deposition was evaluated in eye sections using the fluorescent probe filipin.

Materials and Methods

Mice

The use of animals was in accordance with the ARVO Statement for the Use of Animals in Ophthalmic and Vision Research. French legal and institutional ethics committee review board approvals were obtained.

From the [1]INRA, UMR 1129 FLAVIC, Eye and Nutrition Research Group, F-21000 Dijon, France; the [3]Ocular Neurodegeneration Research Group, Centre for Ophthalmology, Institute for Ophthalmic Research, Eberhard-Karls University, Tübingen, Germany; the [4]Université de Bourgogne, UMR 1129 FLAVIC, Eye and Nutrition Research Group, F-21000 Dijon, France; and the [5]University Hospital, Department of Ophthalmology, F-21000 Dijon, France.

[2]Contributed equally to the work and therefore should be considered equivalent authors.

Submitted for publication July 2, 2007; revised November 14 and December 21, 2007; accepted February 27, 2008.

Disclosure: **L. Bretillon**, None; **N. Acar**, None; **M.W. Seeliger**, None; **M. Santos**, None; **M.A. Maire**, None; **P. Juanéda**, None; **L. Martine**, None; **S. Grégoire**, None; **C. Joffre**, None; **A.M. Bron**, None; **C. Creuzot-Garcher**, None

The publication costs of this article were defrayed in part by page charge payment. This article must therefore be marked "*advertisement*" in accordance with 18 U.S.C. §1734 solely to indicate this fact.

Corresponding author: Lionel Bretillon, INRA, Unité FLAVIC–Equipe Œil et Nutrition, 17 rue Sully, BP 86510, 21065 Dijon cedex, France; lionel.bretillon@dijon.inra.fr.

B6129SF2/J and transgenic apoB100,LDLR$^{-/-}$ mice were purchased from Jackson Laboratories (Bar Harbor, ME), mated, bred, and maintained under controlled conditions of temperature (22 ± 1°C), hygrometry (55%–60%), and light (lights on 7 AM–7 PM, 18 lux) until the age of 7 and 14 months (animal breeding house; INRA, Dijon, France). The mice were fed a standard low-fat diet (128S; Harlan-Teklad, Gannat, France).

Electroretinographic Evaluation

Before ERG recording and fundus examination, the mice were anesthetized by SC injection of ketamine (66.7 mg/kg body weight; Ketanest; Parke-Davis, Berlin, Germany) and xylazine (11.7 mg/kg body weight; Rompun; Bayer Vital, Leverkusen, Germany), and their pupils were dilated with tropicamide eye drops (Mydriaticum Stulln; Pharma Stulln, Nabburg, Germany).

Fundus Photography

In vivo black-and-white images of the fundus were obtained by angiography (Heidelberg Retina Angiograph [HRA]; Heidelberg Engineering GmbH, Heidelberg, Germany), as described elsewhere.[16] The HRA is a confocal scanning laser ophthalmoscope (SLO) that uses different lasers deflected by a mirror oscillating sinusoidally at a frequency up to 20 Hz. Reflectance images of the fundus were acquired using the infrared diode laser (810 nm) and the argon green laser (514 nm). Variation of the focus of the laser beam allowed visualization of the different layers of the fundus (i.e., retina versus RPE). The size of the square scan field was set to 20° × 20° and 10° × 10°. Autofluorescence was excited by the argon blue wavelength (488 nm).

SLO Angiography

Retinal and choroidal vasculature changes were evaluated as described elsewhere[16] after an SC injection of 1% fluorescein (0.25 mL/30 g body weight) and 0.4% ICG (0.5 mL/30 g body weight). The retinal and choroidal vessels began filling approximately 30 seconds after administration. Although timing varied due to variable rates of SC absorption, single pictures, and depth scan movies were taken an average time of 5 to 10 minutes after dye administration. Pictures from the retinal and the choroidal vasculature were recorded with two lasers of the angiograph: an argon blue laser (488 nm) for excitation during fluorescein angiography and an infrared diode laser (795 nm) for excitation during ICG angiography. Barrier filters at 500 and 810 nm provided the optimal cutoff at the respective peak fluorescence emission values for the two types of angiography. The size of the square scan field was set to 20° × 20° and 10° × 10°.

Electroretinograms

ERGs were obtained according to previously described procedures.[17] Mice were dark-adapted overnight before the experiments. After anesthesia, their pupils were dilated with tropicamide (Mydriaticum Stulln; Pharma Stulln) and phenylephrine (Neosynephrin-POS 5%; Usapharm, Saarbrücken, Germany). Silver needle electrodes served as reference (forehead) and ground (tail) electrodes, and gold-wire ring electrodes as active electrodes. The ERG equipment consisted of a Ganzfeld bowl, a DC amplifier, and a computer-based control and recording unit (Toennies Multiliner Vision; Taeger/Toennies, Höchberg, Germany). ERGs were recorded from both eyes simultaneously after the mice were placed in the Ganzfeld bowl. Band-pass filter cutoff frequencies were 0.1 and 3000 Hz for single-flash and flicker-stimuli recordings, respectively.

Single-flash recordings were obtained under both dark-adapted (scotopic) and light-adapted (photopic) conditions. Stimuli were presented with increasing intensities, reaching from 10^{-4} to 25 cd-s/m^2, divided into 10 steps of 0.5 and 1 log cd-s/m^2. Ten responses were averaged with an interstimulus interval of 5 seconds (for 10^{-4}, 10^{-3}, 10^{-2}, 3×10^{-2}, 10^{-1}, and 3×10^{-1} cd-s/m^2) or 17 seconds (for 1, 3, 10, and 25 cd-s/m^2). Light adaptation was accomplished with a background illumination of 30 mcd-s/m^2 presented for 10 minutes to reach the stable level of the photopic response.[18] Amplitudes as a function of flash intensity were fit with a nonlinear saturating function (the Naka-Rushton equation) to obtain values of R_{max} (a maximum response amplitude parameter) and log σ (a sensitivity parameter that represents the flash intensity that produces one-half the maximum response amplitude).

Analysis of the Visual Cycle Retinoids

All procedures with retinoids, from the euthanizing of the animals to analysis, were performed under red illumination to avoid photoisomerization and degradation of the retinoids. Fourteen-month-old apoB100,LDLR$^{-/-}$ and control mice were dark-adapted for 24 hours before death. The eyes were enucleated within 30 seconds after decapitation. Whole mouse eyes (six per analysis) were homogenized in 1.5 mL of 0.1 M MOPS (pH 6.5), 0.2% SDS, and 10 mM NH_2OH in a glass–glass homogenizer and incubated for 30 minutes at room temperature to allow retinal oximes to form. Retinoids were then extracted twice with 4 mL hexane after the addition of 1 mL ethanol. After centrifugation at 900*g* for 2 minutes, the upper phases were collected, dried under nitrogen gas, and resuspended in 150 μL hexane. Retinoids (50 μL) were injected onto a silica HPLC column (250 × 4.6 mm ID, 5 μm; Intertsil Si; Varian, Les Ulis, France) equilibrated with hexane. Retinoids were resolved in hexane-ethyl acetate (90:10, vol/vol) at a flow rate of 1 mL/min. The absorbance of the effluent was monitored simultaneously at 325 nm (for retinols and retinyl esters) and 357 nm (for retinal oximes). Retinyl esters were separated with methanol on a reversed-phase HPLC column (250 × 4.6 mm ID, 5 μm; Nucleosil C-18; Varian) and detected at 325 nm. Retinoids were identified by comparison with commercial standards of retinyl laurate, retinyl myristate, retinyl palmitate, retinyl stearate, all-*trans* retinol, 13-*cis*-retinal and all-*trans* retinal (Sigma-Aldrich, St. Quentin Fallavier, France).

Eye Section Preparation

Seven- and 14-month-old mice were killed, blood samples were taken, and the eyes were enucleated and embedded in a cryoprotectant resin (Cryomount, Thermo-Shandon, Pittsburgh, PA). For further detection of unesterified (UC) and esterified (EC) cholesterol, the eyes were serially sectioned at 8 μm, dried overnight at room temperature, and stored at −80°C until used. For morphometric analyses, the eyes were sectioned sagittally at 20 μm so that the entire eye from the ora serrata to the optic nerve was visible. Sections were fixed 10 minutes in acetone and stored at −20°C until used.

Filipin Histochemistry for Detecting UC and EC

Cholesterol was revealed in eye sections ($n = 4$ in each strain of mice at each age, five sections per eye) with filipin,[19,20] a fluorescent probe that specifically binds the 3β-hydroxy group of cholesterol, according to a protocol described by others.[3,7] Sections for determination of UC were hydrated and incubated for 30 minutes in a filipin solution consisting of 5 mg of filipin (Sigma-Aldrich) dissolved in 1 mL of dimethylformamide and diluted in 100 mL of phosphate-buffered saline. Sections for determination of EC were processed as follows: Native UC was first extracted by two 5-minute rinses in 70% ethanol, and native EC was then hydrolyzed with cholesterol esterase (EC 3.1.1.13; Sigma-Aldrich) at a concentration of 1.65 U/mL in 0.1 M potassium phosphate buffer (pH 7.4), for 3 hours at 37°C. UC newly released by the hydrolysis of EC was then stained with filipin, as just described. Sections incubated with the enzyme vehicle served as the control. The sections were viewed by epifluorescence microscopy with a 420-nm excitation filter and 520-nm barrier filter.

Morphometric Analysis

To determine the thickness of the outer nuclear layer (ONL), we stained the sections with hematoxylin and eosin (Mayer Hematoxylin, Harris Gill Hematoxylin II PAP I, 1:1, vol/vol; Labonord, Templemars, France). The sections that contained the optic nerve were bright-field imaged with a microscope (Eclipse E400; Nikon, Champigny-sur-Marne, France) at 10× power and photographed with a 3 CCD color

video camera (KY-F55E, JVC; Victor Company of Japan, Tokyo, Japan). Digital images were analyzed on computer to measure the thickness of the different layers of the retina ($n = 3$ measurements taken between

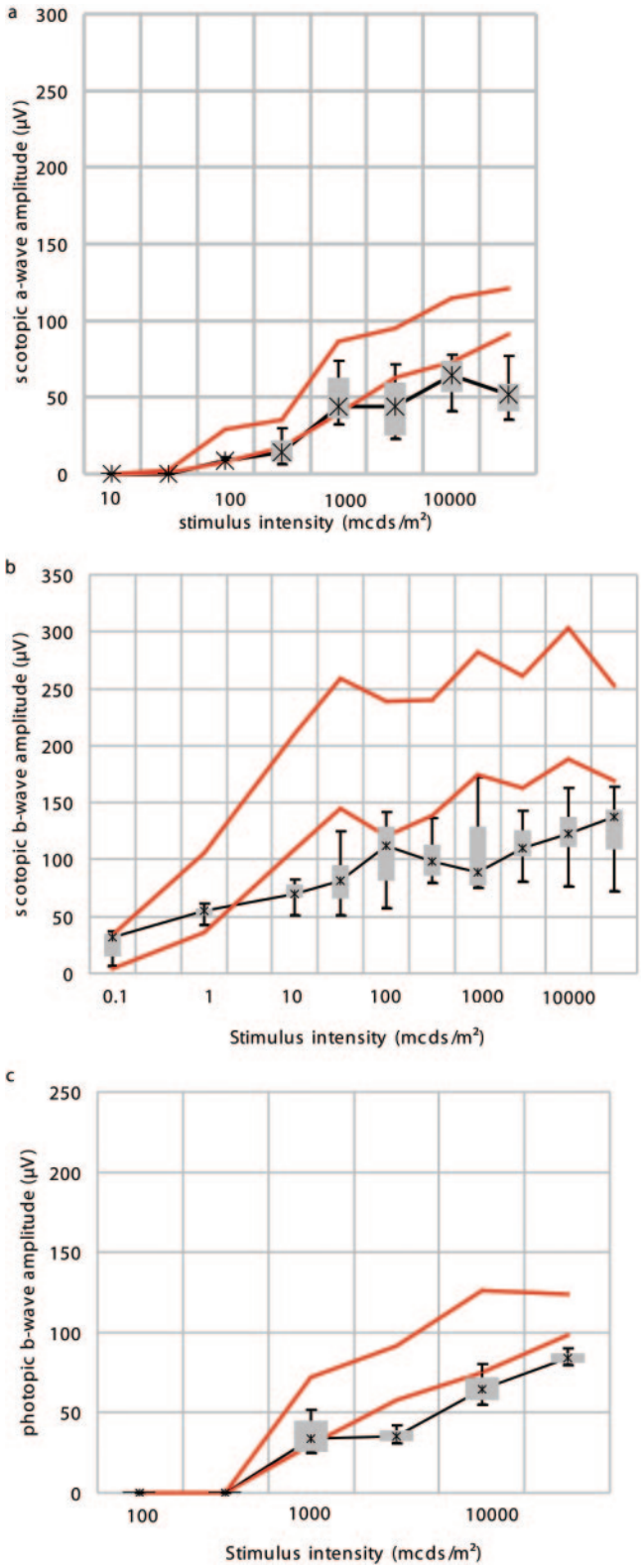

FIGURE 1. Electroretinographic data from 7-month-old control and apoB100,LDLR$^{-/-}$ mice. Dark-adapted (**a**) a- and (**b**) b-wave amplitudes and (**c**) light-adapted b-wave amplitude from apoB100,LDLR$^{-/-}$ mice are plotted as a function of the flash intensity. *Red lines*: normal range given by the 5% and 95% quantile of the control mice ($n = 6$).

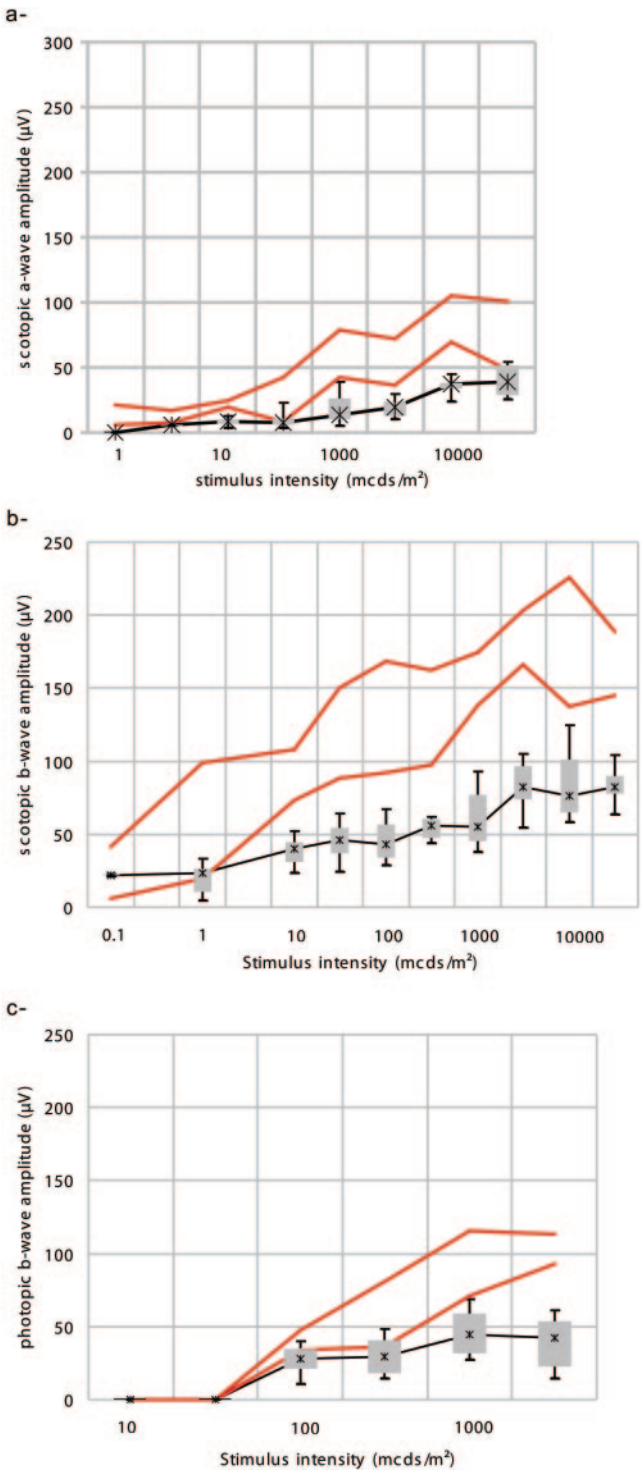

FIGURE 2. Electroretinographic data from 14-month-old control and apoB100,LDLR$^{-/-}$ mice. Dark-adapted (**a**) a- and (**b**) b-wave amplitudes and light-adapted b-wave amplitude (**c**) from apoB100,LDLR$^{-/-}$ mice are plotted as a function of the flash intensity. *Red lines*: normal range given by the 5% and 95% quantile of the control mice ($n = 6$).

0.300 and 0.700 mm from the optic nerve, from four eyes in each strain of animals; Optimas 6.5; IPS, North Reading, MA). Data were analyzed by a standard *t*-test procedure (SAS software; SAS Institute, Cary, NC). Differences were considered significant at $P < 0.05$.

Fatty Acid Profile Analysis of the Retina

At the ages of 7 and 14 months, the mice were euthanized, the eyes enucleated, and the neural retina removed and stored in chloroform-

methanol (2:1, vol/vol). Lipids were extracted,[21] and fatty acids were transmethylated according to Morrison and Smith.[22] Fatty acid methyl esters were analyzed by gas chromatograph (5890 series II; Hewlett-Packard, Palo Alto, CA) equipped with a split/splitless injector, a flame-ionization detector, and a CPSil88-silica capillary column (100 m × 0.25 mm ID, film thickness 0.20 μm; Varian). The injector and the detector were maintained at 250°C and 280°C, respectively. Hydrogen was used as a carrier gas (inlet pressure, 210 kPa). The oven temperature was fixed at 60°C for 1 minute, increased to 85°C at a rate of 3°C/min and then to 190°C at a rate of 20°C/min and left at this temperature for 65 minutes. Fatty acid methyl esters were identified by comparison with commercial standards.

Plasma Levels of Cholesterol

Plasma was obtained from single animals after the collection of whole blood in heparin by aortic puncture at the time of euthanization. Total plasma cholesterol was measured by using an enzymatic procedure. Data were analyzed by a standard two-factor (age, strain) ANOVA procedure (SAS software; SAS Institute). Differences were considered significant at $P < 0.05$.

Results

The apoB100,LDLR$^{-/-}$ mouse serves as an established model for atherosclerotic mechanisms because of the elevation of plasma cholesterol, even in animals fed a standard low-fat diet.[15] We first confirmed this finding, showing that plasma cholesterol was increased threefold in apoB100,LDLR$^{-/-}$ mice compared with the control at 7 (3.3 ± 0.09 and 1.0 ± 0.33 mg/mL, respectively, $n = 6$ in each group $P < 0.0001$,) and 14 months of age (3.7 ± 0.07 mg/mL and 1.2 ± 0.07 mg/mL, respectively, $n = 5$ in each group, $P < 0.0001$).

ERG Response

ERGs were recorded from 7 (Fig. 1)- and 14 (Fig. 2)-month-old control and apoB100,LDLR$^{-/-}$ mice under dark-adapted (Fig. 1a, 1b for 7-month-old mice, Fig. 2a, 2b for 14-month-old mice) and light-adapted (Fig. 1c for 7-month-old mice, Fig. 2c for 14-month-old mice) conditions. Scotopic latencies of both a- and b-waves were unchanged in 7- and 14-month-old apoB100,LDLR$^{-/-}$ mice when compared with control mice at the corresponding age (data not shown). Similarly, under photopic conditions, no delay of b-wave latency was observed (data not shown). The amplitude of a- and b-wave was reduced as a function of time between 7 and 14 months in both strains of mice, and in apoB100,LDLR$^{-/-}$ mice at both ages compared to age-matched control mice (compare Figs. 1a, 2a; Figs. 1b, 2b). The Naka-Rushton representation of the b-wave amplitude as a function of stimulus intensity was used to calculate R_{max} as a parameter for the maximum-response amplitude, and log σ, the sensitivity parameter that represents the flash intensity that produced one half the maximum-response amplitude in apoB100,LDLR$^{-/-}$ and control mice at 7 and 14 months of age (Fig. 3). Even though R_{max} in the control mice was nearly twice that in apoB100,LDLR$^{-/-}$ at 7 (208 ± 36 vs. 125 ± 38 μV; Fig. 3a; $P < 0.0001$) and at 14 (162 ± 17 and 83 ± 15 μV; Fig. 3b; $P < 0.0001$) months of age, log σ was similar in 7-month-old animals (2.5 log units; Fig. 3a) but 0.5 log unit lower in 14-month-old mice than in control animals (1.5 vs. 2 log units; Fig. 3b). These data suggest the loss of rod and cone sensitivity in apoB100,LDLR$^{-/-}$ mice, compared with control mice, after 14 months of age only.

SLO Evaluation

Fundus autofluorescence at 488 nm is suitable to detect fluorophores like lipofuscin in retinal and RPE cells[23] and presumably lipids.[16] A variable degree of autofluorescent dots were present in the apoB100,LDLR$^{-/-}$ mice (Figs. 4a, 4b), but not in the control animals (Fig. 4c). Both retinal and choroidal vasculature were evaluated by SLO after injection of fluorescein and indocyanine green dyes, respectively.[16] Increased autofluorescence in a large number of perivascular cells (Fig. 4d) was present in all apoB100,LDLR$^{-/-}$ mice but not in the control mice, whereas the vascular structure in the 514-nm surface image (Fig. 4e) and the fluorescein angiography (Fig. 4f) at 488 nm did not show any abnormalities.

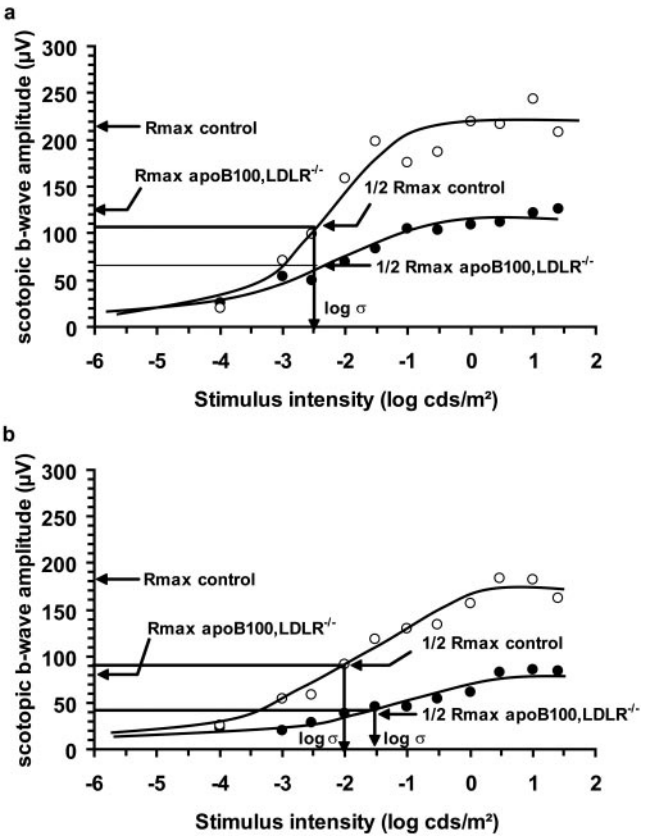

Figure 3. Scotopic b-wave amplitude in (**a**) 7- and (**b**) 14-month-old apoB100,LDLR$^{-/-}$ (●) and control (○) mice as a function of stimulus intensity. The Naka-Rushton representation gives access to R_{max}, the maximum response amplitude parameter, and log σ, the sensitivity parameter that represents the flash intensity that produces one half the maximum response amplitude.

Fatty Acid Composition of the Neural Retina

Fatty acid composition of the neural retina is of major concern for retinal function, as depicted in studies showing that docosahexaenoic acid (DHA) enhances the kinetics of the photocycle by interacting with rhodopsin[24–26] and that DHA depletion lowers the electroretinographic response.[27,28] Nevertheless, control and apoB100,LDLR$^{-/-}$ mice had similar retinal fatty acid profiles with comparable DHA levels (32.0% ± 0.76% in control mice, $n = 3$, versus 32.8% ± 0.39% in apoB100,LDLR$^{-/-}$ mice, $n = 4$, at 14 months of age; 31.8% ± 1.53% in control mice, $n = 3$, vs 31.7% ± 0.56% in apoB100,LDLR$^{-/-}$ mice, $n = 4$, at 7 months of age), which does not explain the reduced ERG response.

Detection of UC and EC in Eye Sections

UC and EC were detected by using filipin in eye sections of both control and apoB100,LDLR$^{-/-}$ mice at 7 and 14 months. UC appeared to be broadly distributed throughout the retina of both control and apoB100,LDLR$^{-/-}$ mice (Figs. 5a, 5c, 5e, 5g). The most striking difference between apoB100,LDLR$^{-/-}$ and

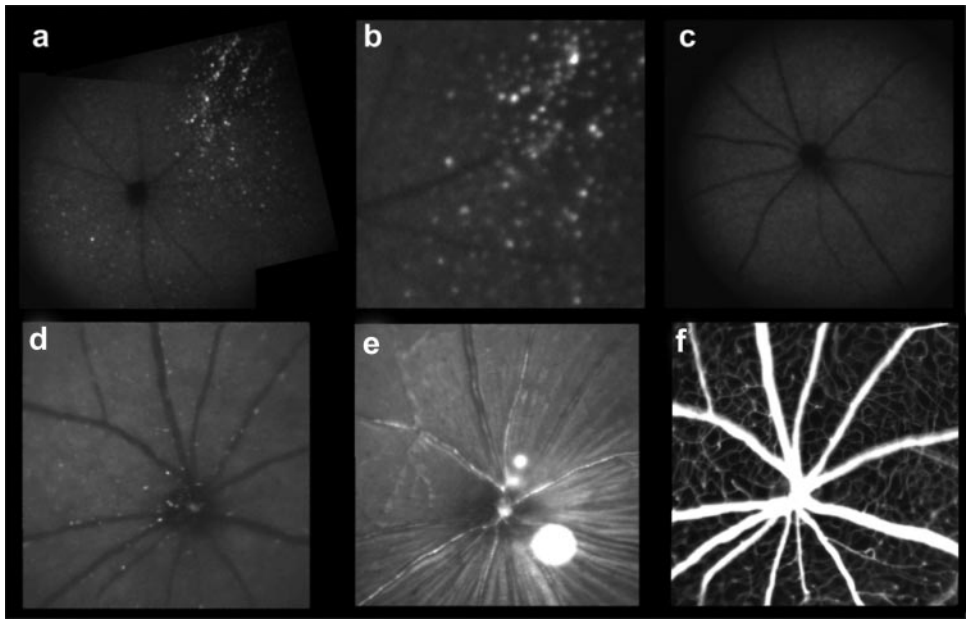

FIGURE 4. Assessment of autofluorescence in apoB100,LDLR$^{-/-}$ mice with SLO. Autofluorescent native images were taken at 488 nm from 14-month-old apoB100,LDLR$^{-/-}$ (**a**, **b** at higher magnification) and control mice (**c**). Perivascular cells were observed at 488 nm in all apoB100,LDLR$^{-/-}$ mice (**d**). The vascular structure was analyzed in 14-month-old apoB100,LDLR$^{-/-}$ mice in the 514-nm surface image (**e**) and after fluorescein dye injection at 488 nm (**f**).

control mice was the age-related accumulation of EC in apoB100,LDLR$^{-/-}$ at 7 months and to a greater extent at 14 months (Figs. 5b versus 5d, 5f versus 5h). Intense laminar fluorescence of EC was found at the basement of the RPE (Figs. 5d, 5h, 5i). On the contrary, 7- and 14-month-old control mice displayed similar low EC staining (Figs. 5b, 5f).

Morphometric Analysis of the Retina

The mean thickness of the outer layers of the retina in apoB100,LDLR$^{-/-}$ mice was comparable to that in control animals (outer segments [OS]: 40.8 ± 7.9 μm compared with 33.5 ± 4.7 μm; ONL: 54.7 ± 8.1 μm compared with 57.1 ± 11.9 μm, respectively, in 14-month-old mice, $P > 0.05$).

DISCUSSION

This report describes a correlation between a dysregulation of the lipid metabolism triggered by the exclusive expression of the human apoB100 gene in the LDL knockout mouse and a reduced ERG response, indicating a functional impairment.

As lipids are major components of the retina and account for up to 50% of rod outer segment membrane dry matter,[29] a change in fatty acid status may be etiologically involved in the reduction of the ERG response. In particular, the interaction between rhodopsin and fatty acids may be relevant, since rhodopsin and DHA colocalize in the outer segments of photoreceptors.[30,31] DHA is recognized as a key factor in the visual function by creating tight associations with rhodopsin that may facilitate the transition to its active form and enhance the kinetics of the photocycle.[24–26,30] Investigators in numerous studies have reported reduced ERG-wave amplitude in DHA-depleted animals.[27,28,32–34] A degeneration of rods and cones would lead to low content in DHA and rhodopsin in the neural retina and thinning of the outer layers of the retina (OS and ONL) that were not observed in our study. Consequently, our data showing reduced ERG in old apoB100,LDLR$^{-/-}$ mice cannot be explained by this type of DHA–rhodopsin mechanism, since no DHA depletion was reported in the retina of these animals, and no differences in the thickness of the OS and ONL were observed between control and apoB100,LDLR$^{-/-}$ mice. Similarly, the age-dependent reduction of b-wave amplitude in both control and apoB100,LDLR$^{-/-}$ mice does not correlate with a loss of DHA in the retina.

Hyperlipemia in the null mice may also contribute to the lower ERG response. Recent clinical data from a single patient showed that hyperlipemia was associated with lipemia retinalis and reduced ERG, although no signs of vascular abnormalities were observed. In this patient, the ERG response returned to normal when hyperlipemia was corrected.[35] The authors hypothesized that the presence of large lipid-rich particles in the blood may produce a turbid serum appearance that would reduce the light intensity reaching the photoreceptors and consequently decrease the ERG response. This potential mechanism remains improbable in our model, since one would expect a- and b-wave latencies to increase concomitantly with the turbidity of the ocular fluids. However, no such delay was observed in apoB100,LDLR$^{-/-}$ mice (data not shown), which discredits the involvement of hyperlipemia, per se.

Far fewer data are available on the role of cholesterol in ERG. Cholesterol was found to form nonspecific interactions with rhodopsin in vitro,[25] which we assume to have only a slight and inconsistent effect on the retinoid cycle. Indeed, like others,[3,36,37] we reported only low content of free cholesterol in the outer segment of the neural retina, which renders the effect of any interaction between cholesterol and rhodopsin highly putative. Moreover, this mechanism remains improbable even in 14-month-old apoB100,LDLR$^{-/-}$ mice since, although cholesteryl ester deposition was observed at the basement of RPE of these animals (Fig. 5), no increase in free cholesterol was found in the outer segments.

We presume the abnormal lipid metabolism in the retina of apoB100,LDLR$^{-/-}$ mice is involved in the accumulation of cholesteryl ester at the basement of RPE. The apoB100,LDLR$^{-/-}$ mouse is an established model for atherosclerosis, in that it shares close features with atherosclerosis in humans: enhanced plasma cholesterol concentrations, aortic fatty streaks,[15] presence of LDL that is almost the exclusive form of cholesterol transport in plasma,[38] and the exclusive expression of human apoB100. Apo-B100 is a large protein that is produced in the liver, where it is assembled into VLDL and remains present in LDL. A commonly recognized role for apoB100 is its capacity to bind LDLR, thereby facilitating internalization of cholesteryl esters from LDL into peripheral cells. The expression of apoB100 in the retina of apoB100,LDLR$^{-/-}$ mice remains to be shown. Nevertheless, we expect apoB100 to be mainly present in circulating lipoproteins and possibly in the choriocapillaris,

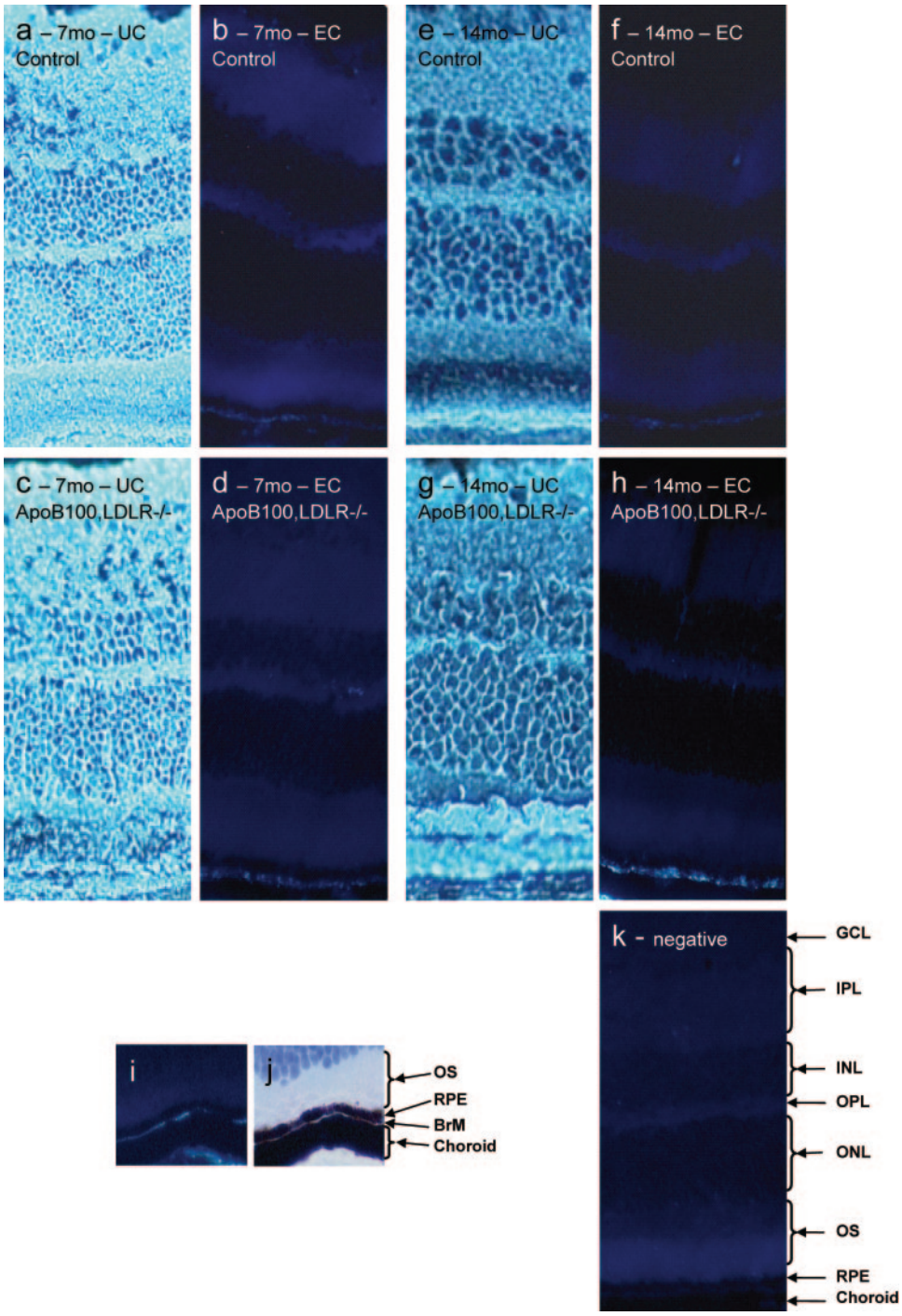

FIGURE 5. Filipin fluorescence of UC (**a**, **c**, **e**, **g**) and EC (**b**, **d**, **f**, **h**, **i**) in sections of 7- and 14-month-old apoB100,LDLR$^{-/-}$ (**c**, **d**, **g**, **h**, **i**) and control (**a**, **b**, **e**, **f**) mouse eyes. EC clearly accumulated in a diffuse pattern at the basement of the RPE (**d**, **h**, **i**). Filipin epifluorescence (**i**) and a bright-field (**j**) section through the outer retinas of apoB100,LDLR$^{-/-}$ mice demonstrating the localization of EC between the RPE and BrM. (**k**) A control negative eye section incubated with ethanol is presented for comparison. GCL, ganglion cell layer; IPL, inner plexiform layer; INL, inner nuclear layer; OPL, outer plexiform layer.

as has been reported.[2,39,40] Assuming that LDL can reach RPE[40,41] and LDLR is present in RPE,[41] the lack of LDLR in apoB100,LDLR$^{-/-}$ animals may abrogate the transfer of cholesterol from circulating LDL into RPE cells, leading to cholesterol deposition. Apart from the interaction of LDLR and apoB100 as a pathway for the transfer of lipid and nutrients to the outer retina, other mechanisms may be suggested, as indicated by the presence of CD36 in the RPE.[39] This pathway may be an alternative route for lipid and nutrients to cross the RPE barrier and target the outer retina, in addition to the lack of LDLR, and may explain the non-null ERG response in apoB100,LDLR$^{-/-}$ mice, as well as why DHA was not reduced in the neural retina of apoB100,LDLR$^{-/-}$ mice, since one would expect low DHA levels if lipid transfer from the RPE to the neural retinal was impaired.

Cholesteryl ester deposition at the basement of the RPE (Fig. 5) may contribute to fundus autofluorescence under laser excitation at 488 nm (Fig. 4). Indeed although lipofuscin remains the dominant autofluorescent entity,[23,42] other lipid deposits may also be detectable in vivo by SLO, in particular in conjunction with OS degradation.[16] Further work is needed to investigate the nature of these deposits, especially the presence of lipofuscin in apoB100,LDLR$^{-/-}$ mice.

The autofluorescent perivascular cells (Fig. 4) may be remnants of vitreous vessel walls that have vanished during the course of ocular development.[43] Alternatively, based on their location in the vicinity of inner retinal vessels, these may be lipid-rich smooth muscles cells or pericytes and would correspond to foam cells observed in major aortic vessels during atherosclerosis. Such an explanation remains probable and

accounts for the fact that that we, like others,[15] observed fatty streaks in thoracic aorta of these animals (data not shown) and that apoB100,LDLR$^{-/-}$ is recognized as a relevant mouse model for atherosclerosis.[15]

Accumulation of lipids under the RPE and within BrM is one of the features of aging[1,2] and AMD.[3,44] AMD is the leading cause of blindness in the elderly in the United States and Western countries.[45,46] Various factors have been associated with AMD, including genetics, environmental factors, aging, cardiovascular disease, and risk factors for cardiovascular disease.[44,46–49] The mechanisms underlying this phenomenon are being actively investigated, but remain partially resolved. Meanwhile, the consequences for the retinal cycle are poorly described. Using an animal model characterized by systemic lipid dysfunction triggered by exclusive apoB100 expression and LDLR invalidation, we were able to describe cholesteryl ester deposition in the retina, together with a reduced ERG response. The present apoB100,LDLR$^{-/-}$ mouse, the LDLR$^{-/-}$ mouse,[9] and the transgenic apoE4 mouse[50] currently are the only models with neutral lipid deposits at the basement of the RPE that can potentially be useful in studying the mechanisms of lipid deposition that occurs universally in the aging human retina.

Acknowledgments

The authors thank Linda Northrup (PhD, ELS, English Solutions, Voiron, France) for the English-language editing of the manuscript, Martine Genty (INRA Dijon, France) for editing the figures, and Christine A. Curcio (University of Alabama at Birmingham) for critical discussion of the manuscript.

References

1. Curcio CA, Millican CL, Bailey T, Kruth HS. Accumulation of cholesterol with age in human Bruch's membrane. *Invest Ophthalmol Vis Sci*. 2001;42:265–274.
2. Malek G, Li CM, Guidry C, Medeiros NE, Curcio CA. Apolipoprotein B in cholesterol-containing drusen and basal deposits of human eyes with age-related maculopathy. *Am J Pathol*. 2003;162:413–425.
3. Curcio CA, Presley JB, Malek G, Medeiros NE, Avery DV, Kruth HS. Esterified and unesterified cholesterol in drusen and basal deposits of eyes with age-related maculopathy. *Exp Eye Res*. 2005;81:731–741.
4. Moore DJ, Hussain AA, Marshall J. Age-related variation in the hydraulic conductivity of Bruch's membrane. *Invest Ophthalmol Vis Sci*. 1995;36:1290–1297.
5. Li CM, Presley JB, Zhang X, et al. Retina expresses microsomal triglyceride transfer protein: implications for age-related maculopathy. *J Lipid Res*. 2005;46:628–640.
6. Cousins SW, Espinosa-Heidmann DG, Alexandridou A, Sall J, Dubovy S, Csaky K. The role of aging, high fat diet and blue light exposure in an experimental mouse model for basal laminar deposit formation. *Exp Eye Res*. 2002;75:543–553.
7. Dithmar S, Sharara NA, Curcio CA, et al. Murine high-fat diet and laser photochemical model of basal deposits in Bruch membrane. *Arch Ophthalmol*. 2001;119:1643–1649.
8. Green WR. Histopathology of age-related macular degeneration. *Mol Vis*. 1999;5:27.
9. Rudolf M, Winkler B, Aherrahou Z, Doehring LC, Kaczmarek P, Schmidt-Erfurth U. Increased expression of vascular endothelial growth factor associated with accumulation of lipids in Bruch's membrane of LDL receptor knockout mice. *Br J Ophthalmol*. 2005;89:1627–1630.
10. Curcio CA, Millican CL. Basal linear deposit and large drusen are specific for early age-related maculopathy. *Arch Ophthalmol*. 1999;117:329–339.
11. Ishibashi S, Goldstein JL, Brown MS, Herz J, Burns DK. Massive xanthomatosis and atherosclerosis in cholesterol-fed low density lipoprotein receptor-negative mice. *J Clin Invest*. 1994;93:1885–1893.
12. Callow MJ, Verstuyft J, Tangirala R, Palinski W, Rubin EM. Atherogenesis in transgenic mice with human apolipoprotein B and lipoprotein (a). *J Clin Invest*. 1995;96:1639–1646.
13. Purcell-Huynh DA, Farese RV Jr, Johnson DF, et al. Transgenic mice expressing high levels of human apolipoprotein B develop severe atherosclerotic lesions in response to a high-fat diet. *J Clin Invest*. 1995;95:2246–2257.
14. Espinosa-Heidmann DG, Sall J, Hernandez EP, Cousins SW. Basal laminar deposit formation in APO B100 transgenic mice: complex interactions between dietary fat, blue light, and vitamin E. *Invest Ophthalmol Vis Sci*. 2004;45:260–266.
15. Sanan DA, Newland DL, Tao R, et al. Low density lipoprotein receptor-negative mice expressing human apolipoprotein B-100 develop complex atherosclerotic lesions on a chow diet: no accentuation by apolipoprotein(a). *Proc Natl Acad Sci USA*. 1998;95:4544–4549.
16. Seeliger MW, Beck SC, Pereyra-Munoz N, et al. In vivo confocal imaging of the retina in animal models using scanning laser ophthalmoscopy. *Vision Res*. 2005;45:3512–3519.
17. Jaissle GB, May CA, Reinhard J, et al. Evaluation of the rhodopsin knockout mouse as a model of pure cone function. *Invest Ophthalmol Vis Sci*. 2001;42:506–513.
18. Peachey NS, Goto Y, al-Ubaidi MR, Naash MI. Properties of the mouse cone-mediated electroretinogram during light adaptation. *Neurosci Lett*. 1993;162:9–11.
19. Kruth HS. Localization of unesterified cholesterol in human atherosclerotic lesions: demonstration of filipin-positive, oil-red-O-negative particles. *Am J Pathol*. 1984;114:201–208.
20. Kruth HS. Histochemical detection of esterified cholesterol within human atherosclerotic lesions using the fluorescent probe filipin. *Atherosclerosis*. 1984;51:281–292.
21. Folch J, Lees M, Sloane Stanley GH. Simple method for the isolation and purification of total lipids from animal tissues. *J Biol Chem*. 1957;226:497–509.
22. Morrison WL, Smith LM. Preparation of fatty acids methyl esters and dimethylacetals from lipids with boron fluoride methanol. *J Lipid Res*. 1964;5:600–608.
23. Delori FC, Dorey CK, Staurenghi G, Arend O, Goger DG, Weiter JJ. In vivo fluorescence of the ocular fundus exhibits retinal pigment epithelium lipofuscin characteristics. *Invest Ophthalmol Vis Sci*. 1995;36:718–729.
24. Bush RA, Malnoe A, Reme CE, Williams TP. Dietary deficiency of N-3 fatty acids alters rhodopsin content and function in the rat retina. *Invest Ophthalmol Vis Sci*. 1994;35:91–100.
25. Grossfield A, Feller SE, Pitman MC. A role for direct interactions in the modulation of rhodopsin by Ω-3 polyunsaturated lipids. *Proc Natl Acad Sci USA.* 2006;103:4888–4893.
26. Pitman MC, Grossfield A, Suits F, Feller SE. Role of cholesterol and polyunsaturated chains in lipid-protein interactions: molecular dynamics simulation of rhodopsin in a realistic membrane environment. *J Am Chem Soc*. 2005;127:4576–4577.
27. Acar N, Chardigny JM, Bonhomme B, Almanza S, Doly M, Sebedio JL. Long-term intake of trans (n-3) polyunsaturated fatty acids reduces the b-wave amplitude of electroretinograms in rats. *J Nutr*. 2002;132:3151–3154.
28. Weisinger HS, Vingrys AJ, Sinclair AJ. Effect of dietary n-3 deficiency on the electroretinogram in the guinea pig. *Ann Nutr Metab*. 1996;40:91–98.
29. Fliesler SJ, Anderson RE. Chemistry and metabolism of lipids in the vertebrate retina. *Prog Lipid Res*. 1983;22:79–131.
30. Niu S-L, Mitchell DC, Lim S-Y, et al. Reduced G protein-coupled signaling efficiency in retinal rod outer segments in response to n-3 fatty acid deficiency. *J Biol Chem*. 2004;279:31098–31104.
31. Yeagle PL. The structures of G-protein coupled receptors. In: Yeagle PL, ed. *The Structure of Biological Membranes*. Boca Raton, FL: CRC Press; 2005:479–498.
32. Diau GY, Loew ER, Wijendran V, Sarkadi-Nagy E, Nathanielsz PW, Brenna JT. Docosahexaenoic and arachidonic acid influence on preterm baboon retinal composition and function. *Invest Ophthalmol Vis Sci*. 2003;44:4559–4566.

33. Heinemann KM, Waldron MK, Bigley KE, Lees GE, Bauer JE. Long-chain (n-3) polyunsaturated fatty acids are more efficient than alpha-linolenic acid in improving electroretinogram responses of puppies exposed during gestation, lactation, and weaning. *J Nutr*. 2005;135:1960–1966.
34. Jeffrey BG, Mitchell DC, Gibson RA, Neuringer M. n-3 fatty acid deficiency alters recovery of the rod photoresponse in rhesus monkeys. *Invest Ophthalmol Vis Sci*. 2002;43:2806–2814.
35. Lu CK, Chen SJ, Niu DM, Tsai CC, Lee FL, Hsu WM. Electrophysiological changes in lipaemia retinalis. *Am J Ophthalmol*. 2005; 139:1142–1145.
36. Boesze-Battaglia K, Fliesler SJ, Albert AD. Relationship of cholesterol content to spatial distribution and age of disc membranes in retinal rod outer segments. *J Biol Chem*. 1990;265:18867–18870.
37. Caldwell RB, McLaughlin BJ. Freeze-fracture study of filipin binding in photoreceptor outer segments and pigment epithelium of dystrophic and normal retinas. *J Comp Neurol*. 1985;236:523–537.
38. Veniant MM, Sullivan MA, Kim SK, et al. Defining the atherogenicity of large and small lipoproteins containing apolipoprotein B100. *J Clin Invest*. 2000;106:1501–1510.
39. Li CM, Chung BH, Presley JB, et al. Lipoprotein-like particles and cholesteryl esters in human Bruch's membrane: initial characterization. *Invest Ophthalmol Vis Sci*. 2005;46:2576–2586.
40. Tserentsoodol N, Sztein J, Campos M, et al. Uptake of cholesterol by the retina occurs primarily via a low density lipoprotein receptor-mediated process. *Mol Vis*. 2006;12:1306–1318.
41. Gordiyenko N, Campos M, Lee JW, Fariss RN, Sztein J, Rodriguez IR. RPE cells internalize low-density lipoprotein (LDL) and oxidized LDL (oxLDL) in large quantities in vitro and in vivo. *Invest Ophthalmol Vis Sci*. 2004;45:2822–2829.
42. Marmorstein AD, Marmorstein LY, Sakaguchi H, Hollyfield JG. Spectral profiling of autofluorescence associated with lipofuscin, Bruch's membrane, and sub-RPE deposits in normal and AMD eyes. *Invest Ophthalmol Vis Sci*. 2002;43:2435–2441.
43. Saint-Geniez M, D'Amore PA. Development and pathology of the hyaloid, choroidal and retinal vasculature. *Int J Dev Biol*. 2004;48: 1045–1058.
44. Abdelsalam A, Del Priore L, Zarbin MA. Drusen in age-related macular degeneration: pathogenesis, natural course, and laser photocoagulation-induced regression. *Surv Ophthalmol*. 1999;44:1–29.
45. Fine SL, Berger JW, Maguire MG, Ho AC. Age-related macular degeneration. *N Engl J Med*. 2000;342:483–492.
46. Vingerling JR, Dielemans I, Bots ML, Hofman A, Grobbee DE, de Jong PT. Age-related macular degeneration is associated with atherosclerosis. The Rotterdam Study. *Am J Epidemiol*. 1995;142: 404–409.
47. Chaine G, Hullo A, Sahel J, et al. Case-control study of the risk factors for age related macular degeneration. France-DMLA Study Group. *Br J Ophthalmol*. 1998;82:996–1002.
48. Smith W, Assink J, Klein R, et al. Risk factors for age-related macular degeneration: pooled findings from three continents. *Ophthalmology*. 2001;108:697–704.
49. Mares-Perlman JA, Brady WE, Klein R, VandenLangenberg GM, Klein BE, Palta M. Dietary fat and age-related maculopathy. *Arch Ophthalmol*. 1995;113:743–748.
50. Malek G, Johnson LV, Mace BE, et al. Apolipoprotein E allele-dependent pathogenesis: a model for age-related retinal degeneration. *Proc Natl Acad Sci USA*. 2005;102:11900–11905.